

Quantum photonic frequency processor on thin-film lithium niobate

Ran Yang,^{1,*} Wei Zhou,^{1,*} Dong-Jie Guo,^{1,*} Hong-Ming Ke,¹ Linrunde Tao,¹ Ying Wei,¹ Jia-Chen Duan,¹ Yu Cui,¹ Kumpeng Jia,¹ Zhenda Xie,¹ Zhongjin Lin,^{2,†} Xinlun Cai,^{2,3} Yan-Xiao Gong,^{1,3,‡} and Shi-Ning Zhu¹

¹*National Laboratory of Solid State Microstructure,
School of Physics, School of Electronic Science and Engineering,
Jiangsu Key Laboratory of Quantum Information Science and Technology,
and Collaborative Innovation Center of Advanced Microstructures, Nanjing University, Nanjing 210093, China*

²*State Key Laboratory of Optoelectronic Materials and Technologies,
School of Electronics and Information Technology,
Sun Yat-sen University, Guangzhou 510275, China*

³*Hefei National Laboratory, Hefei 230088, China*

The rapid development of photonic quantum information processing necessitates precise and programmable control over optical frequency, a capability critical not only for achieving photon indistinguishability but also for exploiting a virtually unbounded frequency dimension. However, efficient and scalable processing of frequency-encoded photon states remains challenging, primarily due to the limited nonlinear optical interaction in most photonic materials. Here, by harnessing the high-performance thin-film lithium niobate electro-optic (EO) platform, we demonstrate an integrated quantum photonic frequency processor that enables coherent and programmable control of photon frequency with high precision. We establish a scalable architecture for frequency-encoded quantum information processing. Using a fully integrated photonic chip, we realize a universal set of frequency-encoded quantum logic gates, including arbitrary single-qubit rotation gates and the two-qubit controlled-phase gate. Furthermore, we demonstrate its application in high fidelity characterization of frequency-bin entangled states. Our work reveals the unprecedented potential of utilizing the frequency degree of freedom in integrated quantum photonic systems.

Introduction

The frequency degree of freedom (DOF) plays a crucial role in optical information processing across both classical [1] and quantum [2] regimes. As an inherently continuous DOF, optical frequency can be discretized to create ultrahigh-dimensional quantum state spaces in a single photon or optical mode, offering a powerful route towards scalable quantum systems. Significant advances have been made in the generation of both large-scale multipartite continuous-variable [3–7], and high-dimensional photonic frequency-bin entangled states [8–13]. However, linear optics confines operations on the frequency DOF to passive separating, mixing, and phase adjustment of frequency modes, preventing genuine cross-mode operations that typically require nonlinear optics. Consequently, the scope of frequency-encoded quantum information processing is more constrained in comparison to more versatile DOFs such as polarization, spatial or path. Hence, to unlock the potential of frequency-encoded quantum technologies, it is crucial to develop fully scalable, robust, and reconfigurable photonic frequency control devices [14, 15].

The fast-driven electro-optic modulation (EOM), typically based on lithium niobate (LN) [16, 17], provides a convenient and programmable means to perform fast, clean, and low-loss spectral operations by utilizing standard radio-frequency and microwave electronics. Combined with low-loss waveguides, and high- Q microresonators, high-performance photonic frequency manipu-

lation devices have been developed, such as frequency shifters and beam splitters [18–21], comb generators [22], frequency circulation [23], and spectral control [24–26]. However, when applied to quantum logic gates and computation, the inherent infinite frequency sidebands generated by EOM modulations would extend beyond the designated computation Hilbert spaces, thereby limiting the success probability and fidelity of the logic operations. To address this problem, a framework for scalable frequency-encoded quantum information processing was proposed by cascading pulse-shaper/EOM modules [27]. Despite successful demonstrations of high-fidelity beam splitters and tritters with a single module [28], realizing a complex logic gate like two-qubit controlled-phase gate in this framework requires several cascaded modules, which increase circuit depth, accumulate optical loss, and ultimately limit the fidelity and scalability [29]. Consequently, the realization of more efficient, scalable, and high-fidelity frequency-encoded quantum information-processing architectures remains an outstanding challenge.

Here we present a monolithic and reconfigurable quantum photonic frequency processor chip fabricated on thin-film lithium niobate (TFLN), a promising platform for integrated photonics [30]. A key module is the microwave-driven coupled double resonators (DR), which can realize a tunable beam splitter between two frequency bins with minimal inter-bin crosstalk. The Hong-Ou-Mandel interference between two photons in distinct fre-

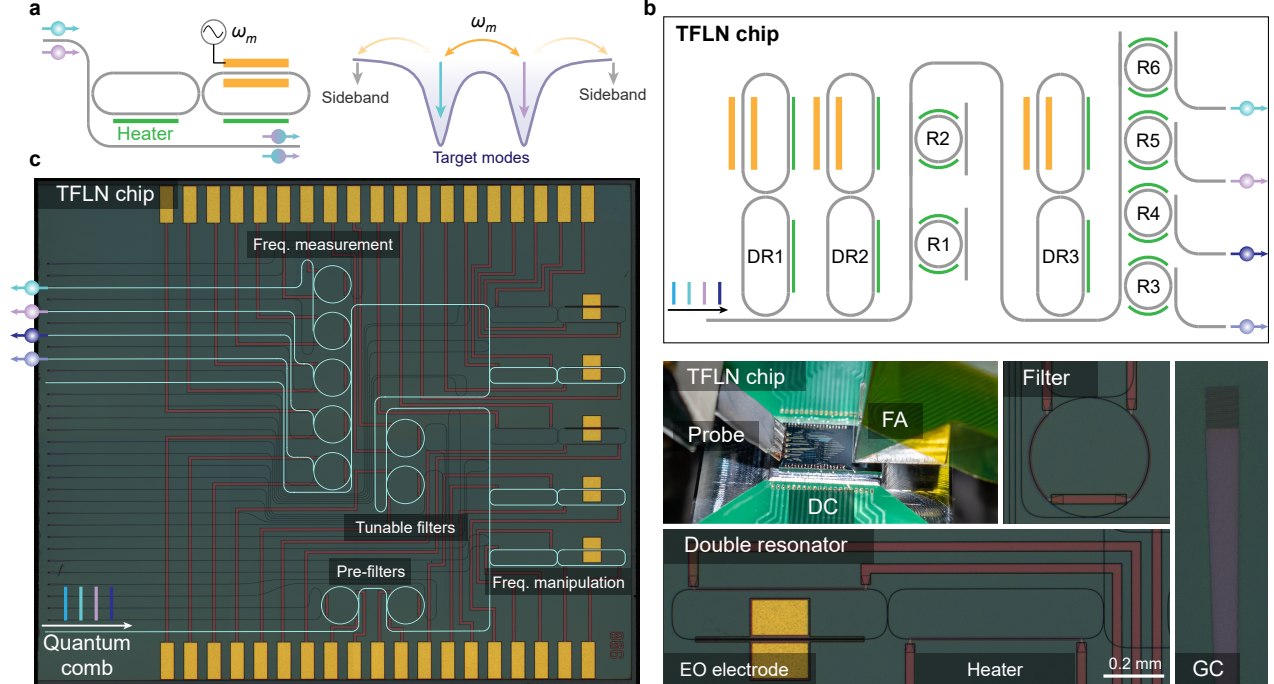


FIG. 1. **Description of the Quantum Photonic frequency processor chip.** **a**, Schematic and operating principle of microwave-driven coupled double resonators (DR). **b**, Schematic diagram of the chip design. **c**, Optical microscope images of the chip and the test setup. FA, fiber array; DC, direct-current source; R, microring resonator; GC, grating coupler.

frequency bins is observed with a visibility of $(94.9 \pm 1.8)\%$. By defining frequency-bin encoded Hilbert spaces, we demonstrate high-quality arbitrary single-qubit rotation logic gates with an average fidelity of $(97.1 \pm 0.6)\%$. Then for the first time, we experimentally realize the canonical ancilla-free linear optical controlled-phase (or equivalently, controlled-Not) gate [31, 32] utilizing frequency-bin encoding, in contrast to previous implementations on other DOFs, such as path [33, 34], polarization [35–37], waveguide mode [38]. The fidelity of this gate is measured to be $(91.4 \pm 1.4)\%$ that could be improved to 98.9%, provided a higher quality photon source. Our approach paves the way for quantum information processing in the continuous frequency DOF, as well as shows a promising way for the seamless integration of frequency-nonidentical photons.

Results

Scheme and device

A schematic of the basic module, a coupled DR, along with its operating principle, is presented in Fig. 1a. When one resonator is driven by a microwave signal with a frequency close to the optical mode splitting of the DR, coherent interconversion between the two frequency modes is induced by the EO effect. Higher-order sidebands are intrinsically suppressed due to the near-zero

density of intra-cavity states at those frequencies. This device functions as a frequency-bin beam splitter (f-BS) acting on two input and two output frequency bins, analogous to a spatial beam splitter (see Supplementary Information Sec. I). Its operation can be described by the unitary matrix U of a standard beam splitter with transmissivity T and reflectivity R , scaled by a total efficiency η (for details, see Supplementary Information Sec. II). Consequently, by controlling the amplitude and phase of microwave driving signals, versatile quantum operations on frequency-bin encoded qubits can be realized.

The schematic diagram of our integrated quantum photonic frequency processor is shown in Fig. 1b. In addition to three DRs, two MRRs, R1 and R2, are used to implement frequency-dependent attenuation in the canonical ancilla-free linear optical controlled-phase gate. Four MRRs, R3, R4, R5, and R6, are employed to separate frequency bins and perform frequency-bin projective measurements. Optical microscope images of the integrated photonic chip are shown in Fig. 1c, which is fabricated based on the 6-inch wafer-scale TFLN technology (see Methods). Grating couplers are used to couple light between on-chip waveguides and fibers with an efficiency of 25% and a bandwidth of 2.5 THz. Two pre-filters are employed to eliminate photons at unwanted frequencies. Note that, there are two other DRs are on the chip,

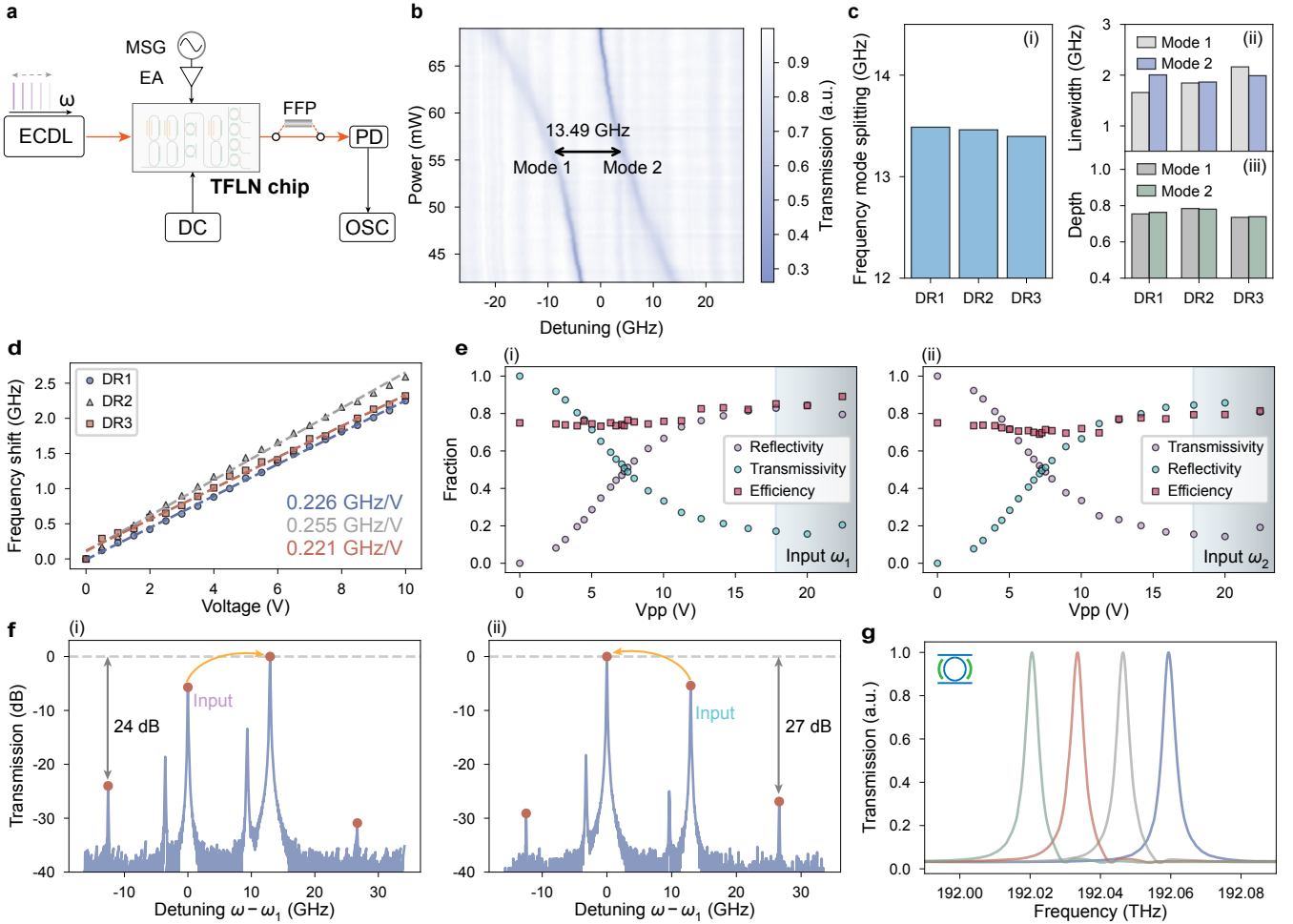


FIG. 2. **Chip characterization.** **a**, Experimental setup for characterizing the chip. ECDL, external cavity diode laser; MSG, microwave signal generator; EA, electrical amplifier; FFP, fiber Fabry-Pérot cavity; PD, photodetector; OSC, oscilloscope. **b**, Transmission spectrum of DR1 against the thermal tuning power. The minimum frequency mode splitting is 13.49 GHz, with balanced transmission of the two modes. **c**, Performance of three DRs, including (i) frequency mode splitting, (ii) linewidth, and (iii) transmission-dip depth. **d**, The resonance shift under DC voltages, with the corresponding EO-response values, obtained from linear fits, listed at lower right corner. **e**, Splitting ratio and total efficiency η of the f-BS for DR1 with input ω_1 (i) and ω_2 (ii). **f**, Frequency distribution at maximal interconversion efficiency, measured by scanning the resonant frequency of a FFP cavity (FSR, 10 GHz). **g**, Transmission spectra of the add-drop microring filters.

which are detuned far from the frequencies used in our experiments.

Chip characterization

We first characterize the performance of each on-chip building block. The experimental setup is illustrated in Fig. 2a. The optical spectroscopy of the resonators is performed by sweeping an external-cavity diode laser (ECDL) across the resonance frequencies. A microwave signal from a microwave signal generator (MSG) is amplified and then applied to the electrodes of DRs to drive the tunable f-BS. The EO responses of the f-BSs are characterized via on-chip MRR filters that selectively separate the frequency components of the output light. A narrow-linewidth fiber Fabry-Pérot (FFP) cavity with a

full width at half maximum (FWHM) of 18 MHz is used to resolve and characterize the higher-order sidebands in high spectral resolution. The output optical signal is detected by a photodetector (PD) and recorded by an oscilloscope (OSC) for further analysis.

By thermally tuning the resonance of the resonator directly coupled to bus waveguide of DR1, we measure the behavior of frequency transmission against thermal power, as shown in Fig. 2b. At the transmission-balanced point, the frequency mode splitting $2g$ is estimated to be 13.49 GHz, which is close to the designed 12.95 GHz that matches the frequency spacing of our quantum comb photon-pair source (see Supplementary Information Sec. III. B). The three DRs, DR1, DR2, and DR3, exhibit consistency in frequency mode split-

ting, resonance linewidth, and dip transmission, as shown in Fig. 2c (i), (ii), and (iii), respectively. Their resonance frequency shifts as a function of a direct-current voltage applied to the inner resonator are presented in Fig. 2d, with the corresponding EO-response values estimated to be 0.226, 0.255, and 0.222 GHz/V, respectively. These modulation efficiencies can be further improved with optimized electrode designs.

To characterize the splitting ratio of the f-BS driven by a microwave signal set at frequency $\omega_m = 12.95$ GHz, we input a continuous wave (CW) laser at frequencies $\omega_1 = 192.02052$ THz and $\omega_2 = 192.03347$ THz, which are symmetrically detuned with respect to the DR doublet shown in Fig. 1a. The measured results of reflectivity and transmissivity for input frequencies ω_1 and ω_2 under different voltages are presented in Fig. 2e (i) and (ii), respectively. Note that the shaded areas indicate the gradual saturation of the electrical amplifiers (EAs). The total efficiency is estimated to exceed 69%, and could be further improved to 97% through optimization of the intrinsic waveguide loss [39, 40]. The higher-order sideband suppression ratios are observed to exceed 24 dB at maximal conversion efficiencies, as shown in Fig. 2f (i) and (ii). This intrinsic suppression ensures closed, low-leakage operations within a well-defined two-frequency-bin subspace, a key requirement for scalable quantum circuits. The two unlabeled peaks come from resonant modes associated with another orthogonal polarization in the FFP cavity. The microring filters are designed with a free spectral range (FSR) of 100 GHz, which in principle support an unambiguous discrimination of four frequency-bins spanning 3×12.95 GHz involved in our quantum experiments. The measured linewidths of the filters are approximately 4 GHz (Fig. 2g), ensuring measurement crosstalk between nearest bins less than 3%. The on-chip efficiency of the filters is estimated at over 94.6%.

Frequency-domain photonic interferences

The operation of the f-BS on single photons can be modeled as a unitary matrix U within a two-dimensional Hilbert space spanned by two frequency bins $\{|\omega\rangle, |\omega + \Delta\omega\rangle\}$ with a spacing of $\Delta\omega = 12.95$ GHz. Due to the bandwidth constraints of the grating couplers, these frequency bins can be selected across a wide operational range from 190.1734 THz to 192.6459 THz. The transformation is expressed as:

$$U = \begin{bmatrix} \sqrt{T} & e^{i\theta}\sqrt{R} \\ -e^{-i\theta}\sqrt{R} & \sqrt{T} \end{bmatrix}, \quad (1)$$

where R and T represent the reflectivity and transmissivity, and θ is the relative phase controlled by the microwave drive. By tuning these parameters, the f-BS essentially acts as a reconfigurable single-qubit gate for frequency-encoded states.

To evaluate the functional performance of the TFLN

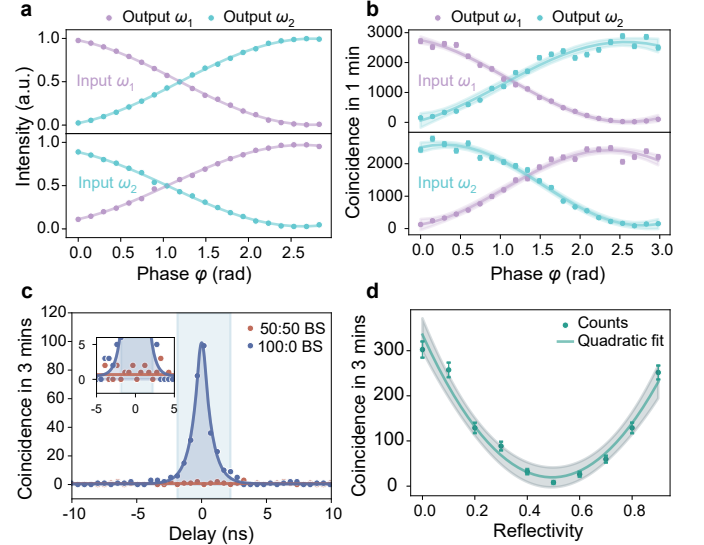


FIG. 3. **Frequency domain photonic interferences.** **a**, Characterization of f-MZI using CW light. **b**, Demonstration of f-MZI using heralded single photon. **c**, Histogram of time-correlated coincidence counts. **d**, Hong-Ou-Mandel interference at different reflectivities.

photonic frequency manipulation system, we first validate the coherence of the f-BS by utilizing a frequency-domain Mach-Zehnder interferometer (f-MZI) configured for two specific frequency bins, ω_1 and ω_2 , with both classical laser light and single-photon state inputs (for details, see Supplementary Information Sec. I). We select DR1 and DR3 shown in Fig. 1b to serve as the two f-BSs in the f-MZI, with the resonances of all other DRs thermally tuned away from the operational frequencies. The resonances of DR1 and DR3 are initialized to be identical, both operating at a 50 : 50 splitting ratio. The phase difference between the two arms in the f-MZI is determined by the relative phase ϕ between two microwave signals, which is tuned by an electrical phase shifter. The two-frequency-bin light is spectrally separated by two MRRs and detected using off-chip power meters.

By injecting a CW laser at frequencies ω_1 and ω_2 , the normalized output intensities at two frequency ports are shown in Fig. 3a, which presents high average visibility $\mathcal{V}_{\text{ave}} = \langle (I_{\text{max}} - I_{\text{min}}) / (I_{\text{max}} + I_{\text{min}}) \rangle = 97.2\%$ for four curves.

The heralded single photons centered at frequencies ω_1 and ω_2 with a Lorentzian bandwidth of 202 MHz are generated from the spontaneous parametric down-conversion (SPDC) inside a monolithic cavity with a FSR of 12.95 GHz (see Supplementary Information Sec. III. B). After passing through the f-MZI, the output photons are routed to off-chip superconducting nanowire single-photon detectors (SNSPDs). The coincidence counts are recorded by a time-correlated single photon counting (TCSPC) module. The measured results are pre-

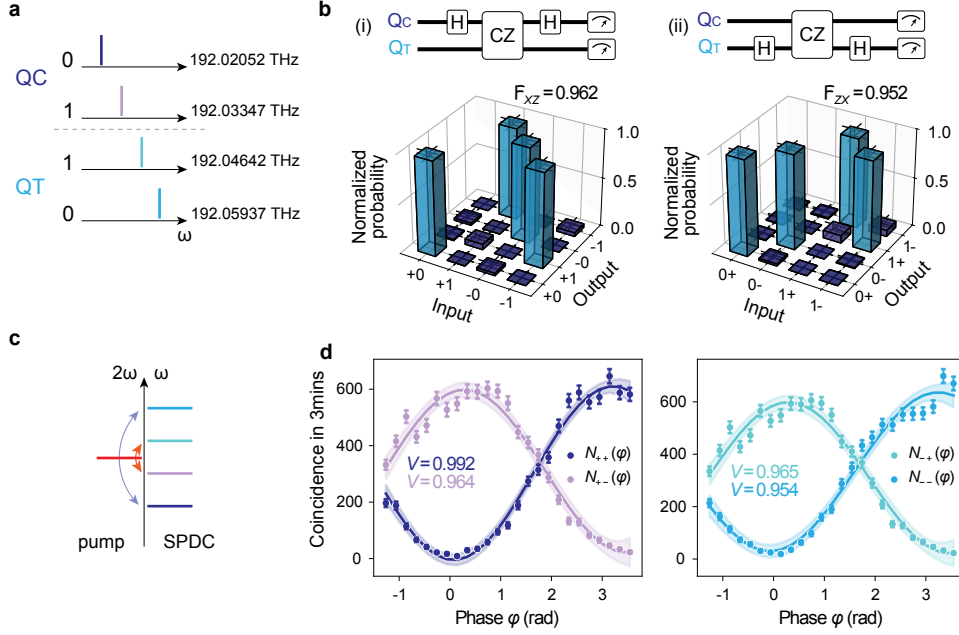


FIG. 4. **Frequency qubits manipulation.** **a**, Encoding of qubits in photonic frequency-bins. **b**, Measured probability distributions of CZ gate with different input states. **c**, Generation of frequency entangled state through SPDC. **d**, Measured entanglement curves.

sented in Fig. 3b, showing a high average visibility of $\mathcal{V}_Q = 97.1 \pm 0.6\%$. This result confirms the ability to achieve high-fidelity and coherent control of frequency-bin photonic states.

Then, we perform the Hong-Ou-Mandel (HOM) interference, a fundamental building block in photonic quantum information processing, between two photons in distinct frequency bins. A pair of photons at frequencies ω_1 and ω_2 generated from SPDC are coupled into the TFLN chip. We employ DR3 as the f-BS in the HOM interferometer for its widest splitting-ratio range among the three DRs (see Fig. S9 in Supplementary Information Sec. III). After frequency separation, the output photons at ω_1 and ω_2 are directed to two separate SNSPDs for detection. Then the coincidence counts are recorded with a time-resolution window of 512 ps. Figure 3c shows the time-correlated coincidence counts with the splitting ratio set at 100:0 and 50:50, respectively. The curves are fitted using a convolution of a two-sided exponential decay function. The result clearly reveals the photon bunching phenomenon in the HOM interference at balanced splitting condition. The visibility of the HOM interference is calculated as $\mathcal{V}_{\text{HOM}} = (N_{\text{max}} - N_{\text{min}})/N_{\text{max}} = 94.9 \pm 1.8\%$ without background count subtraction, where N_{max} and N_{min} denote maximal and minimal counts, respectively. We further measure the HOM interference at different reflectivities of the f-BS, with the experiment results presented in Fig. 3d. These results confirm the capability of the chip for high-visibility nonclassical interference between two photons in distinct frequency bins.

Frequency-bin encoded qubits control

As illustrated in Fig. 4a, four frequency-bins are encoded as the control (Q_C) and target (Q_T) qubits. The chip is configured for implementation and characterization of the ancilla-free linear optical controlled-phase gate [31, 32], or called the CZ gate (see Supplementary Information Sec. II. C). In the circuit, DR2 is tuned to achieve a splitting ratio of $T : R = 1 : 2$ for frequency bins encoded as $|1\rangle_C$ and $|0\rangle_T$. The MRRs R1 and R2 are tuned to introduce an attenuation of 2/3 for photons in state $|0\rangle_C$ and $|1\rangle_T$, respectively. Under this configuration, the frequency-bin encoded CZ gate is constructed. The state preparation is implemented by DR1. The frequency-bin state projection measurements are realized by DR3 and the subsequent MRRs, R3, R4, R5, and R6. We measure the input-output statistics in Pauli basis $XZ(\{| \pm \rangle_c, |0/1\rangle_t\})$ (Fig. 4b(i)) and $ZX(\{|0/1\rangle_c, | \pm \rangle_t\})$ (Fig. 4b(ii)), where DR1 and DR3 are configured to perform the Hadamard operation on either control or target qubit. The lower bound of the quantum process fidelity of the gate can be estimated as $\mathcal{F} \geq (\mathcal{F}_{XZ} + \mathcal{F}_{ZX} - 1) = (91.4 \pm 1.4)\%$ [41], where \mathcal{F}_{XZ} and \mathcal{F}_{ZX} are the fidelity of measured input-output probabilities. The deviation mainly stems from the low coincidence-to-accidental ratio. With a higher quality photon source, the fidelity could be improved to 98.9% (for details, see Supplementary Information Sec. II. C).

We then utilize the device to characterize two photon frequency-bin entanglement. The entangled state $(|00\rangle + |11\rangle)/\sqrt{2}$ is generated from a single-tone CW

pumped SPDC process (Fig. 4c), where only photons in four selected bins are injected into TFLN chip using off-chip filters. By tuning the phase φ of the microwave signal on DR2, the chip is configured to perform projective measurements on superposition states $(|0\rangle \pm |1\rangle)/\sqrt{2}$ and $(|0\rangle \pm e^{-i\varphi}|1\rangle)/\sqrt{2}$ at DR1 and DR2 for two frequency qubits, respectively. The measured coincidence counts for $N_{++}(\varphi)$, $N_{+-}(\varphi)$, $N_{-+}(\varphi)$, and $N_{--}(\varphi)$ are shown in Fig. 4d. The observed average interference visibility of $96.9 \pm 0.6\%$ confirms that frequency-encoded entanglement is preserved with minimal decoherence, highlighting the multifunctional capabilities of our TFLN quantum photonic platform for coherent frequency manipulation.

Conclusions

The ability to coherently manipulate photons in the frequency domain provides a new dimension for scalable quantum information processing. In this work, we have developed an integrated quantum photonic frequency processor on TFLN platform, uniting high-speed EOM with the scalability of integrated photonics. This platform enables programmable frequency-domain operations that serve as universal building blocks for quantum logic, establishing a practical route toward reconfigurable and high-dimensional quantum circuits. Although the CZ gate realized here is non-deterministic, its demonstrated functionalities can be further exploited in more advanced protocols for both continuous-variable and discrete-variable regimes. The frequency processor lays the groundwork for quantum state engineering, spectral multiplexing, and hybrid encoding schemes that coherently integrate frequency, spatial, and polarization modes within a single chip-scale architecture.

In the future, the heterogeneous integration of quantum light sources [42–44], frequency processors, and single-photon detectors [45, 46] will enable fully self-contained quantum photonic systems [47] capable of on-chip quantum state generation, manipulation, and measurement. Such advances will not only eliminate coupling losses and enhance stability, but also realize dense frequency-multiplexed quantum circuits for communication and computation. The continued convergence of integrated electro-optics, nonlinear optics, and quantum state engineering is expected to transform the frequency degree of freedom from a passive carrier into an active, programmable resource for universal quantum information technologies. Moreover, as LN waveguides are well-suited for developing quantum integrated circuits [48, 49], our approach hold great promise integrated in quantum photonic chips.

Acknowledgments

This research is supported by Quantum Science and Technology-National Science and Technology Major Project (Grant Nos. 2021ZD0301500, and

2021ZD0300700), National Key Research and Development Program of China (Grant No. 2019YFA0705000), Natural Science Foundation of Jiangsu Province (Grant No. BK20243060), Natural Science Foundation of Guangdong Province, China (Grant No. 2025A1515011473), and National Natural Science Foundation of China (Grant Nos. 62288101, 62405382, 62293523, and 11974178).

Author contributions

R.Y. and Y.-X.G. conceived the project. R.Y. and D.-J.G. designed the TFLN chip. Z.L. and X.C. fabricated the device. R.Y., W.Z., D.-J.G., H.K., and L.T. implemented the experiment. R.Y., W.Z., and H.K. performed the data analysis. R.Y., W.Z., and Y.-X.G. wrote the paper with input from all the authors. Y.-X.G. and S.-N.Z. supervised the project. All the authors discussed the results and contributed to the paper.

Competing interests

The authors declare no competing interests.

* These authors contribute equally to this work.

† linzhj56@mail.sysu.edu.cn

‡ gongyanxiao@nju.edu.cn

- [1] T. Fortier and E. Baumann, 20 years of developments in optical frequency comb technology and applications, *Communications Physics* **2**, 153 (2019).
- [2] M. Kues, C. Reimer, J. M. Lukens, W. J. Munro, A. M. Weiner, D. J. Moss, and R. Morandotti, Quantum optical microcombs, *Nature Photonics* **13**, 170 (2019).
- [3] M. Chen, N. C. Menicucci, and O. Pfister, Experimental realization of multipartite entanglement of 60 modes of a quantum optical frequency comb, *Phys. Rev. Lett.* **112**, 120505 (2014).
- [4] J. Roslund, R. M. De Araujo, S. Jiang, C. Fabre, and N. Treps, Wavelength-multiplexed quantum networks with ultrafast frequency combs, *Nature Photonics* **8**, 109 (2014).
- [5] Y. Cai, J. Roslund, G. Ferrini, F. Arzani, X. Xu, C. Fabre, and N. Treps, Multimode entanglement in reconfigurable graph states using optical frequency combs, *Nature communications* **8**, 15645 (2017).
- [6] X. Jia, C. Zhai, X. Zhu, C. You, Y. Cao, X. Zhang, Y. Zheng, Z. Fu, J. Mao, T. Dai, *et al.*, Continuous-variable multipartite entanglement in an integrated microcomb, *Nature* **639**, 329 (2025).
- [7] C. Roh, G. Gwak, Y.-D. Yoon, and Y.-S. Ra, Generation of three-dimensional cluster entangled state, *Nature Photonics* **19**, 526 (2025).
- [8] C. Reimer, M. Kues, P. Roztock, B. Wetz, F. Grazioso, B. E. Little, S. T. Chu, T. Johnston, Y. Bromberg, L. Caspani, D. J. Moss, and R. Morandotti, Generation of multiphoton entangled quantum states by means of integrated frequency combs, *Science* **351**, 1176 (2016).
- [9] M. Kues, C. Reimer, P. Roztock, L. R. Cortés, S. Sciara, B. Wetz, Y. Zhang, A. Cino, S. T. Chu, B. E. Little, *et al.*, On-chip generation of high-dimensional entangled

- quantum states and their coherent control, *Nature* **546**, 622 (2017).
- [10] H. Mahmudlu, R. Johanning, A. Van Rees, A. Khodadad Kashi, J. P. Epping, R. Haldar, K.-J. Boller, and M. Kues, Fully on-chip photonic turnkey quantum source for entangled qubit/qudit state generation, *Nature Photonics* **17**, 518 (2023).
- [11] Z. Xie, T. Zhong, S. Shrestha, X. Xu, J. Liang, Y.-X. Gong, J. C. Bienfang, A. Restelli, J. H. Shapiro, F. N. Wong, *et al.*, Harnessing high-dimensional hyperentanglement through a biphoton frequency comb, *Nature Photonics* **9**, 536 (2015).
- [12] L. Olislager, J. Cussey, A. T. Nguyen, P. Emplit, S. Massar, J.-M. Merolla, and K. P. Huy, Frequency-bin entangled photons, *Phys. Rev. A* **82**, 013804 (2010).
- [13] C. Reimer, S. Sciara, P. Roztockii, M. Islam, L. Romero Cortés, Y. Zhang, B. Fischer, S. Loranger, R. Kashyap, A. Cino, *et al.*, High-dimensional one-way quantum processing implemented on d-level cluster states, *Nature Physics* **15**, 148 (2019).
- [14] H.-H. Lu, M. Liscidini, A. L. Gaeta, A. M. Weiner, and J. M. Lukens, Frequency-bin photonic quantum information, *Optica* **10**, 1655 (2023).
- [15] A. Dutt, A. Mohanty, A. L. Gaeta, and M. Lipson, Non-linear and quantum photonics using integrated optical materials, *Nature Reviews Materials* **9**, 321 (2024).
- [16] A. Parriaux, K. Hammani, and G. Millot, Electro-optic frequency combs, *Advances in Optics and Photonics* **12**, 223 (2020).
- [17] Y. Hu, D. Zhu, S. Lu, X. Zhu, Y. Song, D. Renaud, D. Assumpcao, R. Cheng, C. Xin, M. Yeh, *et al.*, Integrated electro-optics on thin-film lithium niobate, *Nature Reviews Physics* **7**, 237 (2025).
- [18] M. Zhang, C. Wang, Y. Hu, A. Shams-Ansari, T. Ren, S. Fan, and M. Lončar, Electronically programmable photonic molecule, *Nature Photonics* **13**, 36 (2019).
- [19] S. Buddhiraju, A. Dutt, M. Minkov, I. A. Williamson, and S. Fan, Arbitrary linear transformations for photons in the frequency synthetic dimension, *Nature communications* **12**, 2401 (2021).
- [20] Y. Hu, M. Yu, D. Zhu, N. Sinclair, A. Shams-Ansari, L. Shao, J. Holzgrafe, E. Puma, M. Zhang, and M. Lončar, On-chip electro-optic frequency shifters and beam splitters, *Nature* **599**, 587 (2021).
- [21] S. Kapoor, A. Rodek, M. Mikołajczyk, J. Szuniewicz, F. Sośnicki, T. Kazimierzczuk, P. Kossacki, and M. Karpiński, Electro-optic frequency shift of single photons from a quantum dot, *Nanophotonics* **14**, 1775 (2025).
- [22] Y. Hu, M. Yu, B. Buscaino, N. Sinclair, D. Zhu, R. Cheng, A. Shams-Ansari, L. Shao, M. Zhang, J. M. Kahn, *et al.*, High-efficiency and broadband on-chip electro-optic frequency comb generators, *Nature photonics* **16**, 679 (2022).
- [23] J. F. Herrmann, V. Ansari, J. Wang, J. D. Witmer, S. Fan, and A. H. Safavi-Naeini, Mirror symmetric on-chip frequency circulation of light, *Nature Photonics* **16**, 603 (2022).
- [24] M. Karpiński, M. Jachura, L. J. Wright, and B. J. Smith, Bandwidth manipulation of quantum light by an electro-optic time lens, *Nature Photonics* **11**, 53 (2017).
- [25] D. Zhu, C. Chen, M. Yu, L. Shao, Y. Hu, C. Xin, M. Yeh, S. Ghosh, L. He, C. Reimer, *et al.*, Spectral control of nonclassical light pulses using an integrated thin-film lithium niobate modulator, *Light: Science & Applications* **11**, 327 (2022).
- [26] F. Sośnicki, M. Mikołajczyk, A. Golestani, and M. Karpiński, Interface between picosecond and nanosecond quantum light pulses, *Nature Photonics* **17**, 761 (2023).
- [27] J. M. Lukens and P. Lougovski, Frequency-encoded photonic qubits for scalable quantum information processing, *Optica* **4**, 8 (2016).
- [28] H.-H. Lu, J. M. Lukens, N. A. Peters, O. D. Odele, D. E. Leaird, A. M. Weiner, and P. Lougovski, Electro-optic frequency beam splitters and tritters for high-fidelity photonic quantum information processing, *Phys. Rev. Lett.* **120**, 030502 (2018).
- [29] H.-H. Lu, J. M. Lukens, B. P. Williams, P. Imany, N. A. Peters, A. M. Weiner, and P. Lougovski, A controlled-not gate for frequency-bin qubits, *npj Quantum Information* **5**, 24 (2019).
- [30] D. Zhu, L. Shao, M. Yu, R. Cheng, B. Desiatov, C. Xin, Y. Hu, J. Holzgrafe, S. Ghosh, A. Shams-Ansari, *et al.*, Integrated photonics on thin-film lithium niobate, *Advances in Optics and Photonics* **13**, 242 (2021).
- [31] H. F. Hofmann and S. Takeuchi, Quantum phase gate for photonic qubits using only beam splitters and postselection, *Phys. Rev. A* **66**, 024308 (2002).
- [32] T. C. Ralph, N. K. Langford, T. B. Bell, and A. G. White, Linear optical controlled-not gate in the coincidence basis, *Phys. Rev. A* **65**, 062324 (2002).
- [33] J. L. O'Brien, G. J. Pryde, A. G. White, T. C. Ralph, and D. Branning, Demonstration of an all-optical quantum controlled-not gate, *Nature* **426**, 264 (2003).
- [34] A. Politi, M. J. Cryan, J. G. Rarity, S. Yu, and J. L. O'Brien, Silica-on-silicon waveguide quantum circuits, *Science* **320**, 646 (2008).
- [35] N. K. Langford, T. J. Weinhold, R. Prevedel, K. J. Resch, A. Gilchrist, J. L. O'Brien, G. J. Pryde, and A. G. White, Demonstration of a simple entangling optical gate and its use in bell-state analysis, *Phys. Rev. Lett.* **95**, 210504 (2005).
- [36] N. Kiesel, C. Schmid, U. Weber, R. Ursin, and H. Weinfurter, Linear optics controlled-phase gate made simple, *Phys. Rev. Lett.* **95**, 210505 (2005).
- [37] R. Okamoto, H. F. Hofmann, S. Takeuchi, and K. Sasaki, Demonstration of an optical quantum controlled-not gate without path interference, *Phys. Rev. Lett.* **95**, 210506 (2005).
- [38] L.-T. Feng, M. Zhang, X. Xiong, D. Liu, Y.-J. Cheng, F.-M. Jing, X.-Z. Qi, Y. Chen, D.-Y. He, G.-P. Guo, G.-C. Guo, D.-X. Dai, and X.-F. Ren, Transverse mode-encoded quantum gate on a silicon photonic chip, *Phys. Rev. Lett.* **128**, 060501 (2022).
- [39] R. Gao, N. Yao, J. Guan, L. Deng, J. Lin, M. Wang, L. Qiao, W. Fang, and Y. Cheng, Lithium niobate microring with ultra-high q factor above 10^8 , *Chinese Optics Letters* **20**, 011902 (2022).
- [40] X. Zhu, Y. Hu, S. Lu, H. K. Warner, X. Li, Y. Song, L. Magalhães, A. Shams-Ansari, A. Cordaro, N. Sinclair, *et al.*, Twenty-nine million intrinsic q-factor monolithic microresonators on thin-film lithium niobate, *Photonics Research* **12**, A63 (2024).
- [41] H. F. Hofmann, Complementary classical fidelities as an efficient criterion for the evaluation of experimentally realized quantum operations, *Phys. Rev. Lett.* **94**, 160504 (2005).

- [42] G.-T. Xue, Y.-F. Niu, X. Liu, J.-C. Duan, W. Chen, Y. Pan, K. Jia, X. Wang, H.-Y. Liu, Y. Zhang, P. Xu, G. Zhao, X. Cai, Y.-X. Gong, X. Hu, Z. Xie, and S. Zhu, Ultrabright multiplexed energy-time-entangled photon generation from lithium niobate on insulator chip, *Physical Review Applied* **15**, 064059 (2021).
- [43] Z. Ma, J.-Y. Chen, Z. Li, C. Tang, Y. M. Sua, H. Fan, and Y.-P. Huang, Ultrabright quantum photon sources on chip, *Physical Review Letters* **125**, 263602 (2020).
- [44] U. A. Javid, J. Ling, J. Staffa, M. Li, Y. He, and Q. Lin, Ultrabroadband entangled photons on a nanophotonic chip, *Physical Review Letters* **127**, 183601 (2021).
- [45] E. Lomonte, M. A. Wolff, F. Beutel, S. Ferrari, C. Schuck, W. H. Pernice, and F. Lenzini, Single-photon detection and cryogenic reconfigurability in lithium niobate nanophotonic circuits, *Nature communications* **12**, 6847 (2021).
- [46] A. Prencipe, S. Gyger, M. A. Baghban, J. Zichi, K. D. Zeuner, T. Lettner, L. Schweickert, S. Steinhauer, A. W. Elshaari, K. Gallo, *et al.*, Wavelength-sensitive superconducting single-photon detectors on thin film lithium niobate waveguides, *Nano Letters* **23**, 9748 (2023).
- [47] K. Alexander, A. Benyamini, D. Black, D. Bonneau, S. Burgos, B. Burrige, H. Cable, G. Campbell, G. Catalano, A. Ceballos, C.-M. Chang, S. Sen Choudhury, C. J. Chung, F. Danesh, T. Dauer, M. Davis, E. Dudley, P. Er-Xuan, J. Fargas, A. Farsi, C. Fenrich, J. Frazer, M. Fukami, Y. Ganesan, G. Gibson, M. Gimeno-Segovia, S. Goeldi, P. Goley, R. Haislmaier, S. Halimi, P. Hansen, S. Hardy, J. Horng, M. House, H. Hu, M. Jadidi, V. Jain, H. Johansson, T. Jones, V. Kamineni, N. Kelez, R. Koustuban, G. Kovall, P. Krogen, N. Kumar, Y. Liang, N. LiCausi, D. Llewellyn, K. Lokovic, M. Lovelady, V. Riseti Manfrinato, A. Melnichuk, G. Mendoza, B. Moores, S. Mukherjee, J. Munns, F.-X. Musalem, F. Najafi, J. L. O'Brien, J. E. Ortmann, S. Pai, B. Park, H.-T. Peng, N. Penthorne, B. Peterson, G. Peterson, M. Poush, G. J. Pryde, T. Ramprasad, G. Ray, A. Viejo Rodriguez, B. Roxworthy, T. Rudolph, D. J. Saunders, P. Shadbolt, D. Shah, A. Bahgat Shehata, H. Shin, J. Sinsky, J. Smith, B. Sohn, Y.-I. Sohn, G. Son, M. C. M. Souza, C. Sparrow, M. Staffaroni, C. Stavrakas, V. Sukumaran, D. Tamborini, M. G. Thompson, K. Tran, M. Triplett, M. Tung, A. Veitia, A. Vert, M. D. Vidrighin, I. Vorobeichik, P. Weigel, M. Wingert, J. Wooding, and X. Zhou, A manufacturable platform for photonic quantum computing, *Nature* **641**, 876 (2025).
- [48] H. Jin, F. M. Liu, P. Xu, J. L. Xia, M. L. Zhong, Y. Yuan, J. W. Zhou, Y. X. Gong, W. Wang, and S. N. Zhu, On-chip generation and manipulation of entangled photons based on reconfigurable lithium-niobate waveguide circuits, *Physical Review Letters* **113**, 103601 (2014).
- [49] R. J. Chapman, T. Kuttner, J. Kellner, A. Sabatti, A. Maeder, G. Finco, F. Kaufmann, and R. Grange, On-chip quantum interference between independent lithium niobate-on-insulator photon-pair sources, *Physical Review Letters* **134**, 223602 (2025).

Methods

Device design and fabrication

The DRs are designed to have 2 GHz linewidth and 12.95 GHz mode splitting. To suppress high-order mode excitation and maintain sufficient coupling rate, a 1 μm -wide waveguide and Euler curve are utilized to ensure adiabatic mode transition in the bending region. The effective radius of the Euler bend is 90 μm , and the length of the straight region is 567 μm , yielding a free spectral range of approximately 76 GHz. For high filtering efficiency and unambiguous frequency discrimination, the micro ring filters are designed to have 4 GHz linewidth and 100 GHz FSR.

The devices are fabricated using a commercially avail-

able x-cut LNOI 6-inch wafer (NANOLN), with a 600 nm LN thin film, a 4.7 μm buried SiO_2 layer and a 500 μm silicon substrate. First, The optical waveguides and passive devices are then patterned onto the wafer using deep ultraviolet stepper lithography. The LN thin film is then etched with a depth of 300 nm, leaving a 300 nm thick slab layer, using inductively coupled plasma reactive-ion etching process. Subsequently, a 1- μm -thick SiO_2 cladding layer is deposited on the top of the waveguide structures by plasma-enhanced chemical vapor deposition (PECVD). The metal electrodes are defined by patterning polymethyl methacrylate (PMMA) resist, followed by gold deposition on top of the SiO_2 cladding layer and lift-off.